

Observations on Recurrent Loss in the Neural Network Model of a Partial Differential Equation: the Advection-Diffusion Equation*

Jonah A. Reeger [†]

Department of Mathematics and Statistics
US Air Force Institute of Technology, 2950 Hobson Way
Wright-Patterson AFB, OH 45433, USA

March 26, 2025

Abstract

A growing body of literature has been leveraging techniques of machine learning (ML) to build novel approaches to approximating the solutions to partial differential equations. Noticeably absent from the literature is a systematic exploration of the stability of the solutions generated by these ML approaches. Here, a recurrent network is introduced that matches precisely the evaluation of a multistep method paired with a collocation method for approximating spatial derivatives in the advection diffusion equation. This allows for two things: 1) the use of traditional tools for analyzing the stability of a numerical method for solving PDEs and 2) bringing to bear efficient techniques of ML for the training of approximations for the action of (spatial) linear operators. Observations on impacts of varying the large number of parameters in even this simple linear problem are presented. Further, it is demonstrated that stable solutions can be found even where traditional numerical methods may fail.

*This report was prepared as an account of work sponsored by an agency of the United States Government. Neither the United States Government nor any agency thereof, nor any of their employees, make any warranty, express or implied, or assumes any legal liability or responsibility for the accuracy, completeness, or usefulness of any information, apparatus, product, or process disclosed, or represents that its use would not infringe privately owned rights. Reference herein to any specific commercial product, process, or service by trade name, trademark, manufacturer, or otherwise does not necessarily constitute or imply its endorsement, recommendation, or favoring by the United States Government or any agency thereof. The views and opinions of authors expressed herein do not necessarily state or reflect those of the United States Government or any agency thereof.

[†]*Email:* jonah.reeger@afit.edu

1 Introduction

The solution of time-dependent partial differential equations (PDE) is a topic of concern across many application areas. Classical approaches to approximating the solution of many PDEs must balance efficiency, accuracy, and stability of the computed solution in the presence of small perturbations to input data and resulting from operations in floating point arithmetic. Consideration of stability ensures that the behavior of the numerical solution produced by a particular method matches that of an exact solution of a PDE as time increases and without magnifying errors. These approaches often first construct approximations to any linear differential or integral operators involving space-like variables, which are subject to boundary or some other algebraic conditions. Such approximations are usually constructed by either expressing the solution as a linear combination of basis functions, e.g., polynomials, trigonometric polynomials, radial kernels, etc., and substituting these expressions directly into the PDE, or by recasting the problem in a weak form and then projecting the dependent variable(s) onto a basis set (see, e.g., [1] for an exposition on the numerical analysis of traditional methods for solving PDEs). Either way this results in a semi-discrete system of ordinary differential equations (ODEs) that is typically numerically integrated using an appropriate method that considers the stability of the solution.

A growing body of literature has been leveraging techniques of machine learning (ML) to build novel approximations to solutions to PDEs. Broadly, existing methods that pair ML with the solution of PDEs do one of the following:

- mimic the method of lines by typically approximating either the action of the differential operators that are present (usually spatial) with a network model or by approximating the entire right-hand side of the PDE through the evaluation of a network (see, e.g., [2, 3, 4]),
- utilize a network to encapsulate the entire evolution; that is, evaluation of the neural network itself evolves the solution a single time step, removing the need to involve classical numerical integration (see, e.g., [5, 6, 7, 8, 9, 10])

At this time, it is not clear that there are tools available for systematically assessing the stability within these ML approaches. However, it was posited that recurrence in the training of a deep neural network encourage stability in the numerical solution [6]. The purpose of this study is to systematically investigate the impacts of recurrence on the construction of weight sets for approximating the action of (spatial) linear differential operators that are used in the process of solving the advection-diffusion equation.

Recurrent Neural Networks (RNNs) can find their origins in the work of McCulloch and Pitts from 1943 [11], where they considered “nets with circles” allowing

for “reference to past events of infinite degree of remoteness.” Further, Rumelhart, et. al., considered the use of parallel distributed processing in the context of sequential thought processing [12]. These ideas have an intimate connection to initial value problems, whose solutions over time reference past information. Several recent works have considered the connection between Neural Networks and dynamic systems [13, 14, 15, 16] in order to improve the stability, in terms of robustness to perturbations, of the networks for typical tasks (e.g., computer vision, natural language processing, etc.). In this work the opposite task is investigated: utilize the tools of ML, specifically related to RNNs, to construct stable solutions to a time dependent PDE—the advection-diffusion equation. A recurrent network is introduced that matches precisely the evaluation of a multistep method paired with a collocation method for approximating spatial derivatives. This allows for two things: 1) the use of traditional tools for analyzing the stability of a numerical method for solving PDEs and 2) bringing to bear efficient techniques of ML for the training of approximations for the action of (spatial) linear operators.

In order to assist the unfamiliar reader, a comprehensive discussion of the solutions of the advection-diffusion equation, the approximation of the action of linear operators through collocation, the construction of multi-step methods for numerical integration and an introduction to the theory of linear stability of ODEs (and discretized PDEs) is first presented in sections 2 through 5. Then, section 6 relates the numerical solution of a linear PDE to a simple neural network, while section 7 introduces a recurrent loss function and discusses the procedure for its minimization. Next, section 8 explains the computational experiments that were performed to identify conditions where stable numerical solutions of the advection diffusion equation can be generated through minimization of the loss function. Observations of the results of these experiments are presented in sections 9 and 10. Finally, section 11 concludes this work.

2 Asymptotic Behavior of the Advection Diffusion Equation

Consider the problem of determining the P -periodic solution, $u : \mathbb{R} \times [0, T] \rightarrow \mathbb{R}$, of

$$\frac{\partial}{\partial t} u(x, t) = \mathcal{L}u(x, t), \quad x \in \mathbb{R}, \quad t \in (0, T] \quad (1a)$$

$$u(x, 0) = u_0(x), \quad x \in \Omega, \quad (1b)$$

where \mathcal{L} is a linear operator acting with respect to x (e.g., a linear combination of various order partial derivatives with respect to x). In the case of the advection

diffusion equation, which will act as a prototype in this study,

$$\mathcal{L} = -c \frac{\partial}{\partial x} + \nu \frac{\partial^2}{\partial x^2}.$$

This equation has been studied in detail, and comprehensive discussions can be found in many texts on the analysis of PDE (see, e.g., [17] section 6-5). Since

$$\mathcal{L}e^{i\frac{2\pi\omega}{P}x} = \left(-i\frac{2\pi\omega}{P}c - \left(\frac{2\pi\omega}{P}\right)^2 \nu \right) e^{i\frac{2\pi\omega}{P}x},$$

with $i = \sqrt{-1}$ reserved here to represent the imaginary unit, a subset of the eigenvalues of \mathcal{L} is (see, e.g., [18])

$$\left\{ z \in \mathbb{C} : z = -i\frac{2\pi\eta}{P}c - \left(\frac{2\pi\eta}{P}\right)^2 \nu, \eta \in \mathbb{Z} \right\}.$$

Given that functions that are continuous and P -periodic with respect to x can be represented by Fourier series, u can be written as

$$u(x, t) = \sum_{\eta=-\infty}^{\infty} b_{\eta}(t)e^{i\frac{2\pi\eta}{P}x},$$

which is a linear combination of orthogonal eigenvectors of \mathcal{L} . Further, P -periodic solutions to the advection diffusion equation then must satisfy

$$\sum_{\eta=-\infty}^{\infty} \left(\frac{d}{dt}b_{\eta}(t) + \left(i\frac{2\pi\eta}{P}c + \left(\frac{2\pi\eta}{P}\right)^2 \nu \right) b_{\eta}(t) \right) e^{i\frac{2\pi\eta}{P}x} = 0,$$

that is, the time dependent coefficients are defined by

$$b_{\eta}(t) = b_{\eta}(0)e^{-i\frac{2\pi\eta}{P}ct - \left(\frac{2\pi\eta}{P}\right)^2 \nu t}$$

so that

$$u(x, t) = \sum_{\eta=-\infty}^{\infty} b_{\eta}(0)e^{i\frac{2\pi\eta}{P}(x-ct) - \left(\frac{2\pi\eta}{P}\right)^2 \nu t}. \quad (2)$$

Note that $\{b_{\eta}(0)\}_{\eta=-\infty}^{\infty}$ is the set of Fourier series coefficients for the initial data. That is,

$$b_{\eta}(0) = \frac{1}{P} \int_0^P u_0(x) e^{-i\frac{2\pi\eta}{P}x} dx. \quad (3)$$

It is straightforward to show that if P -periodic u (with respect to x) satisfies the conditions that $\frac{\partial^{p-1}}{\partial x^{p-1}}u(x, t)$ is continuous and $\frac{\partial^p}{\partial x^p}u(x, t)$ is piecewise continuous

for each $x \in \mathbb{R}$, then $b_\eta(0) = O(|\eta|^{-p})$ as $\eta \rightarrow \pm\infty$ (see, e.g., [17]). Further, for such u with $p \geq 1$, the convergence implied in (2) is absolute and uniform. The solution (2) translates the initial data with speed c while the amplitude decays relative to the constant ν . That is, when the initial data is bounded, solutions to the advection-diffusion equation are at least bounded as $t \rightarrow \infty$ and will have amplitude that decays if $\nu > 0$.

3 An Approach to Approximating the Action of the Linear Operator

A typical first step in approximating the solution to (1a) is the consideration of spatial derivatives at each location in a given computational node set $\mathcal{S} = \{x_k\}_{k=0}^N \subset \mathbb{R}$. Since u is periodic with period P , it is convenient for \mathcal{S} to be contained entirely in a single period, e.g., $\mathcal{S} \subset [0, P)$. Further, to reduce computational expense, the approximation at each point is constructed using only a set $\mathcal{N}_{k,n} = \{x_{k,j}\}_{j=1}^n$, $n \ll N$, of pairwise distinct points near x_k . For reasons that are discussed later, the value of n is chosen to be odd in this work. It is typical for $\mathcal{N}_{k,n} \subset \mathcal{S}$; however, with the periodicity of u it is useful to artificially extend \mathcal{S} to include two periodic images of the set when selecting information for the local approximations. That is, two additional sets of nodes, $\mathcal{S}^\pm = \{x_k \pm P\}_{k=0}^N$, are artificially introduced and $\mathcal{N}_{k,n}$ is then the set of n points in $\mathcal{S} \cup \mathcal{S}^+ \cup \mathcal{S}^-$ nearest to x_k .

Now, if u has at least n continuous derivatives with respect to the first argument everywhere in Ω , then for each value of t there exists a polynomial interpolant of degree at most $n - 1$ [19]

$$s_k(x, t) = \sum_{j=1}^n \psi_{k,j}(x) u(x_{k,j}, t),$$

that satisfies $s_k(x_{k,j}, t) = u(x_{k,j}, t)$, $j = 1, 2, \dots, n$. The functions $\psi_{k,j}(x)$ are typically Lagrange basis elements constructed on the set $\mathcal{N}_{k,n}$ or some other basis set that satisfies the cardinal property

$$\psi_{k,j}(x_{k,l}) = \begin{cases} 1, & l = j \\ 0, & l \neq j \end{cases}.$$

The action of a linear operator, \mathcal{L} , acting again with respect to x on u is then approximated locally as

$$(\mathcal{L}u)(x, t) \approx (\mathcal{L}s_k)(x, t) = \sum_{j=1}^n (\mathcal{L}\psi_{k,j})(x) u(x_{k,j}, t).$$

Evaluating the local approximation at x_k reveals

$$(\mathcal{L}u)(x_k, t) \approx \sum_{j=1}^n w_{k,j} u(x_{k,j}, t) \quad (4)$$

where $w_{k,j} = (\mathcal{L}\psi_{k,j})(x_k)$. In what follows, it will be assumed that the set \mathcal{S} consists of equally spaced points in $[0, P)$. For instance, a common choice (and the one used herein) is $x_k = kh_x$, $k = 0, 1, \dots, N$, where $h_x = P/(N + 1)$. Further, two useful properties are assumed about each set $\mathcal{N}_{k,n}$:

1. the local computational nodes are arranged in ascending order, i.e., $x_{k,j+1} > x_{k,j}$, $j = 1, 2, \dots, n - 1$, and
2. the distance, $|x_{k,j} - x_k|$, from $x_{k,j}$ to x_k , $j = 1, 2, \dots, n$, is the same for all k .

These assumptions on \mathcal{S} and $\mathcal{N}_{k,n}$ ensure that for typical choices of the basis $\{\psi_{k,j}\}_{j=1}^n$ the weights satisfy for every $k = 1, 2, \dots, N$, $w_{k,j} = w_j$, a value independent of k . Specifically, for the advection-diffusion equation the vector of weights defined entrywise as $[\mathbf{w}]_j = w_j$ can be written as a linear combination of approximations, i.e., $\mathbf{w} = -(c/h_x)\mathbf{w}_1 + (\nu/h_x^2)\mathbf{w}_2$, where the entries of \mathbf{w}_1 and \mathbf{w}_2 are the weights for approximating the actions of $\frac{\partial}{\partial x}$ and $\frac{\partial^2}{\partial x^2}$, respectively, at \mathbf{x}_k (scaled to the case of $h_x = 1$). To simplify what follows, let

$$\boldsymbol{\omega} = \begin{bmatrix} \mathbf{w}_1 \\ \mathbf{w}_2 \end{bmatrix}.$$

For a fixed value of t , it is typical to approximate the action of \mathcal{L} on u at each point in \mathcal{S} simultaneously through the product of an $(N + 1) \times (N + 1)$ matrix, D , with a vector containing values of u evaluated at the nodes in \mathcal{S} . The entries of D are found row by row (something that is easily parallelized). These entries are defined as

$$[D]_{kl} = \begin{cases} w_j & \text{if } x_{k,j} = x_l \text{ or } x_{k,j} = x_l \pm P \text{ for some } (k, j) \\ 0 & \text{otherwise} \end{cases}, \quad (5)$$

that is, entry l of row k is nonzero only if x_l (one of the points in \mathcal{S}) or one of its periodic images, $x_l \pm P$, appears in the set $\mathcal{N}_{k,n}$ of the points nearest x_k . Under the assumptions above placed on \mathcal{S} and $\mathcal{N}_{k,n}$, the matrix D is circulant and sparse and thus has eigenvalues that are easily computed.

Enforcing (1a) at each point in \mathcal{S} and applying the local approximations for the action of \mathcal{L} leads to the semi-discrete system of equations

$$\frac{d}{dt}\mathbf{u}(t) \approx D\mathbf{u}(t) \quad (6)$$

where

$$\mathbf{u}(t) = [u(x_0, t) \quad u(x_1, t) \quad \cdots \quad u(x_N, t)]^T$$

and

$$\frac{d}{dt}\mathbf{u}(t) = [\frac{d}{dt}u(x_0, t) \quad \frac{d}{dt}u(x_1, t) \quad \cdots \quad \frac{d}{dt}u(x_N, t)]^T.$$

Further, given that D is a circulant matrix, for any fixed $\psi \in \mathbb{Z}$, it has orthonormal eigenvectors $\mathbf{v}_{\eta+(N+1)\psi}$, $\eta = -\lfloor N/2 \rfloor, \dots, -1, 0, 1, \dots, \lfloor N/2 \rfloor$, with entries ($k = 0, 1, 2, \dots, N$)

$$[\mathbf{v}_{\eta+(N+1)\psi}]_{k+1} = \frac{1}{\sqrt{N+1}} e^{\frac{2\pi i(\eta+(N+1)\psi)k}{N+1}} = \frac{1}{\sqrt{N+1}} e^{\frac{2\pi i\eta k}{N+1}}$$

and corresponding eigenvalues

$$\lambda_\eta = \sum_{j=-(n-1)/2}^{(n-1)/2} w_{j+(n+1)/2} e^{\frac{2\pi i j \eta}{N+1}}. \quad (7)$$

Therefore, when evaluated at $x_k = kh_x$, $k = 0, 1, \dots, N$, (with $h_x = P/(N+1)$) continuous, P -periodic initial data for (1) with absolutely convergent series (2) can be expressed in the vector

$$\mathbf{u}(0) = \sum_{\eta=-\lfloor N/2 \rfloor}^{\lfloor N/2 \rfloor} \sum_{\psi \in \mathbb{Z}} b_{\eta+(N+1)\psi}(0) \mathbf{v}_{\eta+(N+1)\psi} = \sum_{\eta=-\lfloor N/2 \rfloor}^{\lfloor N/2 \rfloor} \mathbf{v}_\eta \sum_{\psi \in \mathbb{Z}} b_{\eta+(N+1)\psi}(0),$$

with the second equality following from the recognition that $\mathbf{v}_{\eta+(N+1)\psi} = \mathbf{v}_\eta$ for all $\psi \in \mathbb{Z}$. Similarly, the sampled solutions to (1) can be written

$$\mathbf{u}(t) = \sum_{\eta=-\lfloor N/2 \rfloor}^{\lfloor N/2 \rfloor} \mathbf{v}_\eta \beta_\eta(t). \quad (8)$$

with

$$\beta_\eta(t) = \sum_{\psi \in \mathbb{Z}} b_{\eta+(N+1)\psi}(0) e^{-i \frac{2\pi(\eta+(N+1)\psi)}{P} ct - \left(\frac{2\pi(\eta+(N+1)\psi)}{P} \right)^2 \nu t}$$

That is, it is likely (dependent on $b_{\eta+(N+1)\psi}(0)$) that some of $\mathbf{u}(t)$ is in the direction of each of the eigenvectors of D .

4 Time Integration with Multistep Methods

The semidiscrete PDE can be numerically integrated with, for instance, a multistep method as

$$\tilde{\mathbf{u}}(t + h_t) = \tilde{\mathbf{u}}(t) + h_t \sum_{l=0}^{s-1} \alpha_l D \tilde{\mathbf{u}}(t - lh_t), \quad (9)$$

with $h_t > 0$ and the tilde indicating the values of the numerical solution. To simplify the ensuing discussion consider, for now, the scalar ordinary differential equation (ODE)

$$\frac{d}{dt}\mu(t) = f(t, \mu(t)), \quad t > 0 \quad (10a)$$

$$\mu(0) = \mu_0 \quad (10b)$$

the set of coefficients $\{\alpha_l\}_{l=0}^{s-1}$ in (9) is constructed by way of

$$\begin{aligned} \mu(t + h_t) &= \mu(t) + \int_t^{t+h_t} f(\tau, \mu(\tau)) d\tau \\ &\approx \mu(t) + h_t \sum_{l=0}^{s-1} \alpha_l f(t - lh_t, \mu(t - lh_t)), \end{aligned} \quad (11)$$

where

$$\alpha_l = \int_0^1 \prod_{\substack{j=0 \\ j \neq (s-l)}}^{s-1} \frac{\tau + s - (j+1)}{s - l - j} d\tau \quad (12)$$

results from integrating a Lagrange basis polynomial now used in the interpolation of f at the equally spaced values of $t - lh_t$, $l = 0, 1, \dots, s-1$. Consequently, these methods, known as s -step Adams-Bashforth methods (AB- s), are explicit and they are exact when f is a polynomial of degree at most $s-1$ with respect to its first argument. For more generic and sufficiently smooth v , when exact values of $\mu(t - lh_t)$, $l = 0, 1, \dots, s-1$, are known this approximation is $O(h_t^{s+1})$ accurate (in terms of truncation error) for $\mu(t + h_t)$, as $h_t \rightarrow 0$. Considering approximate numerical integration in time, this choice leads to a method given by

$$\tilde{\mu}(t + h_t) = \tilde{\mu}(t) + h_t \sum_{l=0}^{s-1} \alpha_l f(t - lh_t, \tilde{\mu}(t - lh_t)) \quad (13)$$

that is $O(h_t^s)$ accurate [19].

5 Linear Stability

In the further simplified linear case of (10), where $f(t, \mu(t)) = z\mu(t)$ for some scalar $z \in \mathbb{C}$, it is common to analyze for which values of the quantity $h_t z$ the numerical solution of (10) generated by the method (14) match the asymptotic behavior of the exact solution $\mu(t)$ as $t \rightarrow \infty$ (or at least remain bounded).

When z has nonpositive real part, the exact solution to (10), given by $\mu(t) = \mu_0 \exp(zt)$, is bounded and when the real part of z is negative, $\mu(t) \rightarrow 0$ as $t \rightarrow \infty$. In the case of z with positive real part, solutions grow exponentially, which is a difficulty for many numerical methods.

Notice that

$$\tilde{\mu}(t + h_t) = \tilde{\mu}(t) + h_t \sum_{l=0}^{s-1} \alpha_l z \tilde{\mu}(t - lh_t) \quad (14)$$

is a linear recurrence relation. It is helpful to note that this recurrence relation appears as the first equation of the system of linear equations

$$\tilde{\boldsymbol{\mu}}(t + h_t) = M \tilde{\boldsymbol{\mu}}(t).$$

where $\tilde{\boldsymbol{\mu}}(t) = [\tilde{\mu}(t) \quad \tilde{\mu}(t - h_t) \quad \cdots \quad \tilde{\mu}(t - (s-1)h_t)]^T$ and

$$M = \begin{bmatrix} 1 + \alpha_0 h_t z & \alpha_1 h_t z & \alpha_2 h_t z & \cdots & \alpha_{s-2} h_t z & \alpha_{s-1} h_t z \\ 1 & 0 & 0 & \cdots & 0 & 0 \\ 0 & 1 & 0 & \cdots & 0 & 0 \\ & & 0 & \ddots & \vdots & \vdots \\ & & & \ddots & 1 & 0 \\ & & & & 0 & 1 \\ & & & & & 0 \end{bmatrix}.$$

As long as $\tilde{\mu}(jh_t)$, $j = 0, 1, \dots, s-1$, are known values it is straightforward to reason that for $l > 0$

$$\tilde{\boldsymbol{\mu}}((s+l)h_t) = M^{l+1} \tilde{\boldsymbol{\mu}}((s-1)h_t).$$

The matrix M has characteristic polynomial

$$p(\zeta) = (-1)^s (\zeta^s - (1 + \alpha_0 h_t z) \zeta^{s-1} - \sum_{j=1}^{s-1} \alpha_j h_t z \zeta^{s-(j+1)}),$$

whose roots, $\zeta_0, \zeta_1, \dots, \zeta_s$, are the eigenvalues of M . Further,

$$\boldsymbol{\zeta}_j = [\zeta_j^{s-1} \quad \zeta_j^{s-2} \quad \cdots \quad \zeta_j \quad 1]^T$$

is an eigenvector of M associated with the eigenvalue ζ_j . Let $M = W(Z + P)W^{-1}$ be the Jordan form of M where Z is the diagonal matrix with $[Z]_{jj} = \zeta_j$ and P is a nilpotent matrix with $\|P\| = 1$. Then

$$\tilde{\boldsymbol{\mu}}((s+l)h_t) = W(Z + P)^{l+1} W^{-1} \tilde{\boldsymbol{\mu}}((s-1)h_t), \quad l > 0.$$

From this it is clear that $\|\tilde{\boldsymbol{\mu}}((s+l)h_t)\|$ is bounded as l increases if $|\zeta_i| \leq 1$ when ζ_i is a simple root of p or is not defective as an eigenvalue of M and if

$|\zeta_i| < 1$ for a root of greater multiplicity that is defective [20]. Expressing ζ in polar form, evaluation of (as in, e.g., [21])

$$zh = \frac{e^{is\theta} - e^{i(s-1)\theta}}{\sum_{l=0}^{s-1} \alpha_l e^{-i(s-1-l)\theta}}$$

with $\theta \in [0, 2\pi)$ traces a curve in the complex plane, indicating the choices of $\xi = zh_t$ for which $|\zeta| = 1$. The linear stability region corresponds to those where $\|\tilde{\boldsymbol{\mu}}((s+l)h_t)\|$ is bounded.

Returning to the solving (6), since D is unitarily diagonalizable, (9) can be expressed as

$$V^* \tilde{\mathbf{u}}(t + h_t) = V^* \tilde{\mathbf{u}}(t) + h_t \sum_{l=0}^{s-1} \alpha_l \Lambda V^* \tilde{\mathbf{u}}(t - lh_t),$$

with $V = [\mathbf{v}_{-\lfloor N/2 \rfloor}, \dots, \mathbf{v}_{-1}, \mathbf{v}_0, \mathbf{v}_1, \dots, \mathbf{v}_{\lfloor N/2 \rfloor}]$ and Λ the diagonal matrix with $[\Lambda]_{kk} = \lambda_{k-\lfloor N/2 \rfloor-1}$. Therefore, each component of $V^* \tilde{\mathbf{u}}(t)$ should have the asymptotic behavior of the corresponding component of $V^* \mathbf{u}(t)$. Further, it is clear from (8) that for linear stability (considering that solutions to (1) are bounded for the advection diffusion equation) values of h_t such that $h_t \lambda$ is contained in the linear stability region of the method should be sought for each eigenvalue, λ_η , of D .

6 A Network Representation of a Single Step

Departing from traditional approaches to the development of methods for solving (1), the step from t to $t + h_t$ via (9) can alternatively be viewed as the evaluation of a neural network, albeit one with linear activation functions and no bias. A simple schematic of this single step can be seen in figure 6. Under the assumptions that the computational node set is equally spaced and the nodes in $\mathcal{N}_{k,n}$, $k = 1, 2, \dots, N$, are sorted in ascending order, here the network is considered to, instead, have five separate layers to assist in the use of backpropagation to compute the gradients of the cost function defined below.

For $l \geq 0$, the layers are evaluated, in turn, beginning with the input layer. This layer has $N + 1$ nodes which can be represented by the $(N + 1) \times 1$ vector

$$\zeta_\tau^I((s-1+l)h_t; \boldsymbol{\omega}) = \begin{cases} \tilde{\mathbf{u}}((s-1+l)h_t; \boldsymbol{\omega}), & l = 0 \\ \zeta_\tau^+((s-1+l-1)h_t; \boldsymbol{\omega}), & l > 0 \end{cases}.$$

Notice that when $l = 0$, the input layer is simply the value of $\tilde{\mathbf{u}}((s-1)h_t; \boldsymbol{\omega})$. This and the values of $\tilde{\mathbf{u}}(kh_t; \boldsymbol{\omega})$, $k = 0, 1, \dots, s-2$ are assumed to be available to kickstart the method, which is a common requirement for multistep methods. These values could be obtained using a one-step method of appropriate order,

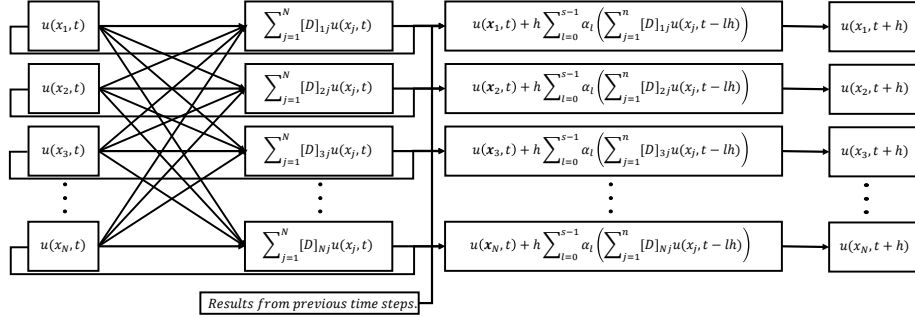


Figure 1: A simplified schematic of a single step of an s -step multistep method for a semi-discrete PDE cast as a network.

such as a Runge-Kutta or Taylor series method. For $l > 0$, the values $\zeta_{\tau}^I((s-1+l)h_t; \omega)$, and so $\zeta_{\tau}^+((s-1+l-1)h_t; \omega)$, are simply values of $\tilde{\mathbf{u}}((s-1+l)h_t; \omega)$ computed by a feedforward pass through the network.

Next, the assignment layer duplicates and arranges the values in $\zeta_{\tau}^I((s-1+l)h_t)$ into the $n(N+1) \times 1$ vector

$$\zeta_{\tau}^A((s-1+l)h_t; \omega) = U \zeta_{\tau}^I((s-1+l)h_t; \omega),$$

with U a constant $n(N+1) \times N+1$ sparse matrix defined by

$$[U]_{ij} = \begin{cases} 1, & x_j \in \mathcal{N}_{k,n} \text{ and } n(k-1) + 1 \leq i \leq nk \\ 0, & \text{otherwise} \end{cases}.$$

The first n entries of $\zeta_{\tau}^A((s-1+l)h_t; \omega)$ are the elements of $\zeta_{\tau}^I((s-1+l)h_t; \omega)$ that correspond to \mathcal{N}_1 (in ascending order), the next n entries are the same for \mathcal{N}_2 , and so on. That is,

$$\zeta_\tau^A((s-1+l)h_t; \boldsymbol{\omega}) = \begin{bmatrix} \tilde{u}(x_{0,1}, (s-1+l)h_t; \boldsymbol{\omega}) \\ \tilde{u}(x_{0,2}, (s-1+l)h_t; \boldsymbol{\omega}) \\ \vdots \\ \tilde{u}(x_{0,n}, (s-1+l)h_t; \boldsymbol{\omega}) \\ \tilde{u}(x_{1,1}, (s-1+l)h_t; \boldsymbol{\omega}) \\ \tilde{u}(x_{1,2}, (s-1+l)h_t; \boldsymbol{\omega}) \\ \vdots \\ \tilde{u}(x_{1,n}, (s-1+l)h_t; \boldsymbol{\omega}) \\ \vdots \\ \tilde{u}(x_{N,1}, (s-1+l)h_t; \boldsymbol{\omega}) \\ \tilde{u}(x_{N,2}, (s-1+l)h_t; \boldsymbol{\omega}) \\ \vdots \\ \tilde{u}(x_{N,n}, (s-1+l)h_t; \boldsymbol{\omega}) \end{bmatrix}.$$

Third, the reshape layer constructs a full $(N+1) \times n$ matrix

$$Z_\tau^R((s-1+l)h_t; \boldsymbol{\omega}) = \sum_{j=1}^n R_j \zeta_\tau^A((s-1+l)h_t; \boldsymbol{\omega}) \mathbf{e}_j^T$$

from the values of $\zeta_\tau^A((s-1+l)h_t; \boldsymbol{\omega})$, with R_j , $j = 1, 2, \dots, n$, a set of constant $(N+1) \times n(N+1)$ sparse matrices containing entries

$$[R_j]_{il} = \begin{cases} 1 & l = (i-1)n + j \\ 0 & \text{otherwise} \end{cases}.$$

Note that $[Z_\tau^R((s-1+l)h_t; \boldsymbol{\omega})]_{kj}$ corresponds to $x_{k,j} \in \mathcal{N}_{k,n}$, i.e.,

$$Z_\tau^R(\cdot; \boldsymbol{\omega}) = \begin{bmatrix} \tilde{u}(x_{0,1}, \cdot; \boldsymbol{\omega}) & \tilde{u}(x_{0,2}, \cdot; \boldsymbol{\omega}) & \cdots & \tilde{u}(x_{0,n}, \cdot; \boldsymbol{\omega}) \\ \tilde{u}(x_{1,1}, \cdot; \boldsymbol{\omega}) & \tilde{u}(x_{1,2}, \cdot; \boldsymbol{\omega}) & \cdots & \tilde{u}(x_{1,n}, \cdot; \boldsymbol{\omega}) \\ \vdots & \vdots & & \vdots \\ \tilde{u}(x_{N,1}, \cdot; \boldsymbol{\omega}) & \tilde{u}(x_{N,2}, \cdot; \boldsymbol{\omega}) & \cdots & \tilde{u}(x_{N,n}, \cdot; \boldsymbol{\omega}) \end{bmatrix}.$$

Next, the convolution layer performs the operation $D\tilde{\mathbf{u}}((s-1+l)h_t; \boldsymbol{\omega})$ through the matrix/vector multiplication defined in

$$\zeta_\tau^C((s-1+l)h_t; \boldsymbol{\omega}) = Z_\tau^R((s-1+l)h_t; \boldsymbol{\omega}) \left(-\frac{c}{h_x} \mathbf{w}_1 + \frac{\nu}{h_x^2} \mathbf{w}_2 \right),$$

so that $\zeta_\tau^C(\cdot; \boldsymbol{\omega})$ is an $N+1 \times 1$ vector when both \mathbf{w}_1 and \mathbf{w}_2 are $n \times 1$ vectors.

Finally, the additive layer evaluates the multistep method (9) by way of

$$\zeta_{\tau}^{+}((s-1+l)h_t; \boldsymbol{\omega}) = \zeta_{\tau}^I((s-1+l)h_t; \boldsymbol{\omega}) + h_t \sum_{j=0}^{s-1} \alpha_j \zeta_{\tau}^C((s-1+l-j)h_t; \boldsymbol{\omega})$$

Note that for $l = 0, 1, \dots, s-1$, this expression relies on the values of $\zeta_{\tau}^C(kh_t; \boldsymbol{\omega})$, $k = 0, 1, \dots, s-1$, which have not been computed. These correspond to the evaluation of $D\tilde{\mathbf{u}}(kh_t; \boldsymbol{\omega})$, which can be completed directly by multiplication or by evaluating in sequence $\zeta_{\tau}^I(kh_t; \boldsymbol{\omega}) = \tilde{\mathbf{u}}(kh_t; \boldsymbol{\omega})$, $\zeta_{\tau}^A(kh_t; \boldsymbol{\omega}) = U\zeta_{\tau}^I(kh_t; \boldsymbol{\omega})$, $Z_{\tau}^R(kh_t; \boldsymbol{\omega}) = \sum_{j=1}^n R_j \zeta_{\tau}^A(kh_t; \boldsymbol{\omega}) \mathbf{e}_j^T$ and $\zeta_{\tau}^C(kh_t; \boldsymbol{\omega}) = Z_{\tau}^R(kh_t; \boldsymbol{\omega}) \left(-\frac{c}{h_x} \boldsymbol{\omega}_1 + \frac{\nu}{h_x^2} \boldsymbol{\omega}_2 \right)$.

The latter is preferred because it more easily highlights the dependence of $\zeta_{\tau}^C(kh_t; \boldsymbol{\omega})$ on the entries of $\boldsymbol{\omega}$ for backpropagation.

A time-stepping method traverses this network many times, with results from each step clearly impacting all later times.

7 Recurrent Loss and Backpropagation

The cost (loss) function considered here is (similar to that of [6])

$$J(\boldsymbol{\omega}) = \sum_{\tau=1}^T \sum_{q=0}^{Q-1} J_{\tau q}(\boldsymbol{\omega}),$$

with

$$J_{\tau q}(\boldsymbol{\omega}) = \frac{1}{2} \left\| \zeta_{\tau}^{+}((s-1+q)h_t; \boldsymbol{\omega}) - \mathbf{u}_{\tau}((s+q)h_t) \right\|_2^2.$$

In this expression for the cost, τ enumerates T separate cases of initial conditions that are used to generate training data, $\mathbf{u}_{\tau}(t)$, and q counts Q time steps beyond the initial s steps required to kickstart the multi-step method beginning at $t = 0$. The intention is to choose $Q > 1$ to promote stability in the solution of the PDE by minimizing the forward error with respect to entries of $\boldsymbol{\omega}$ across multiple steps at once. Due to the small number of decision variables here, a quasi-Newton method (which requires computation of the gradient and Hessian of J with respect to these variables) is favored in determining the extreme points of J . Given a particular value of q , call it q^* , the value of $\zeta_{\tau}^{+}((s-1+q^*)h_t; \boldsymbol{\omega})$ is dependent on all values of $\zeta_{\tau}^{+}((s-1+q)h_t; \boldsymbol{\omega})$ for which $q < q^*$ and so all must be considered, in turn, when computing the gradient (and hessian) of the loss. The results for each value of τ are independent from one another, so when minimizing J it suffices to consider each $J_{\tau q}$ in turn.

As is typical for the computation of the gradient of the objective via backpropagation, it is useful to compute a variety of intermediate quantities that

leverage the chain rule of differentiation. These quantities are summarized in tables 1 and 2, and they can be used to compute the gradients with respect to the weights as

$$\nabla_{\boldsymbol{\omega}} J(\boldsymbol{\omega}) = \begin{bmatrix} -\frac{c}{h_x} I \\ \frac{\nu}{h_x^2} I \end{bmatrix} \sum_{\tau=1}^T \sum_{q=0}^{Q-1} \sum_{l=0}^{s-1+q} Z_{\tau}^R(lh_t; \boldsymbol{\omega}) \delta_{\tau q}^C(lh_t; \boldsymbol{\omega}).$$

The quasi-Newton method attempts to find roots of the gradient of J with respect to the decision variables. Beginning with an initial guess at the weights, $\boldsymbol{\omega}^{(0)}$, the approximations for the roots are updated as

$$\boldsymbol{\omega}^{(\kappa+1)} = \boldsymbol{\omega}^{(\kappa)} + \rho^{(\kappa)} \boldsymbol{\sigma}^{(\kappa)}, \quad (15)$$

with $\rho^{(\kappa)} \in (0, 1]$ a line search parameter and $\boldsymbol{\sigma}^{(\kappa)}$ satisfying

$$H^{(\kappa)} \boldsymbol{\sigma}^{(\kappa)} = -\nabla_{\boldsymbol{\omega}} J^{(\kappa)}(\boldsymbol{\omega}) \Big|_{\boldsymbol{\omega}=\boldsymbol{\omega}^{(\kappa)}}.$$

The superscript in parentheses, with $\kappa = 0, 1, 2, \dots$, in these expressions indicates the iteration, or epoch in the language of neural networks, of the method for minimizing the cost. Therefore, $H^{(\kappa)}$ is meant to represent the Hessian of J (or an approximation thereof) with respect to $\boldsymbol{\omega}$ and evaluated at $\boldsymbol{\omega}^{(\kappa)}$. Instead of computing $H^{(\kappa)}$ exactly at each iteration, which is significantly more expensive than backpropagation for the gradient, the BFGS approximation [22] is utilized instead. The approximate Hessian is initialized as

$$H^{(0)} = \left\| \nabla_{\boldsymbol{\omega}} J(\boldsymbol{\omega}) \Big|_{\boldsymbol{\omega}=\boldsymbol{\omega}^{(0)}} \right\|_2 I$$

I is the identity matrix of appropriate size.

Note that the line search parameter $\rho^{(\kappa)}$ [22] chosen so that

$$J(\boldsymbol{\omega}^{(\kappa)} + \rho^{(\kappa)} \boldsymbol{\sigma}^{(\kappa)}) < J(\boldsymbol{\omega}^{(\kappa)}). \quad (16)$$

At iteration κ , $\rho^{(\kappa)}$ is initialized as one, and J is evaluated at the result of (15). While $J(\boldsymbol{\omega}^{(\kappa)} + \rho^{(\kappa)} \boldsymbol{\sigma}^{(\kappa)}) \geq J(\boldsymbol{\omega}^{(\kappa)})$, $\rho^{(\kappa)}$ is successively decreased by a multiplicative factor of $3/4$. This process continues until (16) is met, at which point $\boldsymbol{\omega}^{(\kappa+1)}$ is assigned by (15). If $\rho^{(\kappa)}$ decreases below a chosen lower bound (here 10^{-5}), then the optimization algorithm is terminated and assumed to have failed.

Given the relationship between \mathbf{w}_1 and \mathbf{w}_2 and the action of \mathcal{L} on a cardinal basis set, minimization of J can be thought of as having a connection to determining a basis for the space of solutions on which the chosen multistep method is stable.

Additive Layer	$\delta_{\tau q}^+((s-1+l)h_t) := \nabla_{\zeta_\tau^+((s-1+l)h_t; \omega)} J_{\tau q}(\omega) = \begin{cases} \zeta_\tau^+((s-1+q)h_t; \omega) - \mathbf{u}_\tau((s+q)h_t), & l = q \\ \delta_{\tau q}^I((s+l)h_t; \omega), & 0 \leq l < q \end{cases}$
Convolution Layer	$\delta_{\tau q}^C((s-1+l)h_t; \omega) := \nabla_{\zeta_\tau^C((s-1+l)h_t; \omega)} J_{\tau q}(\omega) = h_t \sum_{j=0}^{\min(s-1, q-l)} \alpha_j \delta_{\tau q}^+((s-1+l+j; \omega)h_t)$
Reshape Layer	$[\Delta_{\tau q}^R((s-1+l)h_t; \omega)]_{ij} := \frac{\partial}{\partial [Z_\tau^R((s-1+l)h_t; \omega)]_{ij}} J_{\tau q}(\omega) = [\delta_{\tau q}^C((s-1+l)h_t; \omega)]_i \left[-\frac{c}{h_x} \omega_1 + \frac{\nu}{h_x^2} \omega_2 \right]_j$
Assignment Layer	$\delta_{\tau q}^A((s-1+l)h_t; \omega) := \nabla_{\zeta_\tau^A((s-1+l)h_t; \omega)} J_{\tau q}(\omega) = \sum_{j=1}^n R_j^T (\Delta_{\tau q}^R((s-1+l)h_t; \omega) \mathbf{e}_j)$
Input Layer	$\delta_{\tau q}^I((s-1+l)h_t; \omega) := \nabla_{\zeta_\tau^I((s-1+l)h_t; \omega)} J_{\tau q}(\omega) = \delta_{\tau q}^+((s-1+l)h_t; \omega) + U^T \delta_{\tau q}^A((s-1+l)h_t; \omega)$

Table 1: Intermediate quantities useful for backpropagation. These values are computed for each $q = 0, 1, \dots, Q-1$ and for $l = q, q-1, \dots, 0$.

Convolution Layer	$\delta_{\tau q}^C(lh_t; \omega) := \nabla_{\zeta_\tau^C(lh_t; \omega)} J_{\tau q}(\omega) = h_t \sum_{j=s-l}^{\min(s, s+q-l)} \alpha_{j-1} \delta_{\tau q}^+((l+j-1)h_t; \omega)$
-------------------	--

Table 2: Intermediate quantities useful for backpropagation. These values are computed for each $q = 0, 1, \dots, Q-1$ and for $l = s-2, s-3, \dots, 0$.

8 Numerical Experiments

Numerical experiments were performed to investigate the circumstances, given the many possible parameter choices detailed so far, for which the set of weights, $\boldsymbol{\omega}$, determined through the minimization of J lead to stable solutions of (1). Since the decay rate of the coefficients of the Fourier series of the initial data have a correspondence to the differentiability of the initial data, three variations on initial conditions were also considered as a proxy for differing smoothness. That is, for each of $p = 0, 2, 8, T$ cases of initial data are generated via (2) with $b_\eta(0) = b_{-\eta}(0) = \frac{1}{\eta^p} \hat{b}_{\eta,T}$, for $\eta = 0, 1, \dots, (N-1)/2$, and $b_\eta(0) = b_{-\eta}(0) = 0$ otherwise. Here, $\hat{b}_{\eta,T}$ is a value chosen from the random uniform distribution on $(-1, 1)$, and solutions to (1) are given by (2) for all values of $x \in \mathbb{R}$ and $t > 0$.

In this work n is chosen to be an odd number, so that the local node set is centered on x_k , that is, $\mathcal{N}_{k,n} = \{x_k + (-(n-1)/2 + j - 1)h_x\}_{j=1}^n$. Define D' to be the matrix, with eigenvalues λ' , constructed from the second-order centered differences ($n = 3$ with $\psi_{k,j}$ a Lagrange polynomial basis element in (4)) when approximating $\frac{\partial}{\partial x}$ and $\frac{\partial^2}{\partial x^2}$ with periodicity enforced. That is, D' is constructed as in (5) from the weight vector $\boldsymbol{\omega}' = -c/h_x \mathbf{w}'_1 + \nu/h_x^2 \mathbf{w}'_2$, with

$$\mathbf{w}'_1 = \frac{1}{2} \begin{bmatrix} \mathbf{0}_{(n-3)/2}^T & -1 & 0 & 1 & \mathbf{0}_{(n-3)/2}^T \end{bmatrix}^T$$

and

$$\mathbf{w}'_2 = \begin{bmatrix} \mathbf{0}_{(n-3)/2}^T & 1 & 2 & 1 & \mathbf{0}_{(n-3)/2}^T \end{bmatrix}^T.$$

When $\nu = 0$ and $c > 0$ this matrix is antisymmetric, and so has purely imaginary eigenvalues. Alternatively, when $\nu > 0$ and $c = 0$ the matrix D' is symmetric with purely real eigenvalues. Otherwise, the eigenvalues exist on a curve in the left half of the complex plane, with negative real part. Further, the stability region of AB-2 is a closed curve contained entirely in the left half of the complex plane (along with the origin). Therefore, when $\nu = 0$ there is no nonzero value of h_t such that $\lambda' h_t$ is contained in the stability region of the multi-step method. For all other choices of $\nu > 0$, there is a maximum value, denoted $h_{t,N,\nu,s}$, such that $\lambda' h_{t,N,\nu,s}$ is contained in the stability region of AB- s . The value of $h_{t,N,\nu,s}$ is chosen numerically and iteratively utilizing a bisection process that brackets this critical value of h_t and tests which half of the bracket produces eigenvalues contained entirely in the stability region. In the case of $\nu = 0$ and $s = 2$, since there is no such value, $h_{t,N,0,2}$ is set to the value of $h_{t,N,0,3}$. Figure 2 illustrates the stability regions and $\lambda' h_t$ when h_t is set to these critical values for all choices of N , s and ν investigated here. The solid curve, known as the stability boundary, illustrates the boundary of the (shaded) stability region, while the markers (dependent on ν) illustrate the locations of the scaled eigenvalues.

Experiments are performed for values of h_t near these critical values of $h_{t,N,\nu,s}$,

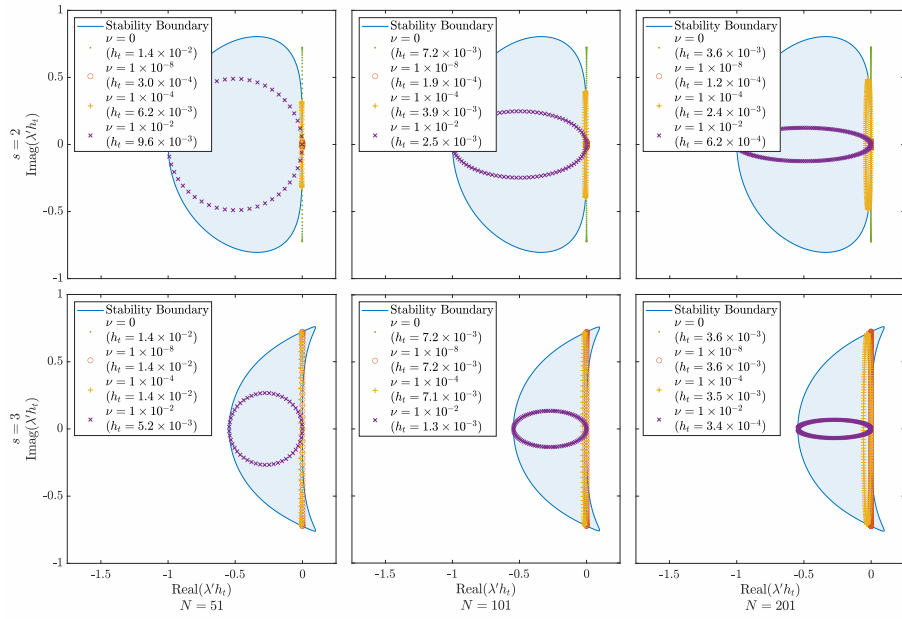


Figure 2: Eigenvalues of D' for various values of ν with $h_t = h_{t,N,\nu,s}$. The value of $h_{t,N,\nu,s}$ is indicated in parentheses for each choice of N , ν and s . The stability region (shaded) of AB- s is shown with its stability boundary outlined by a solid curve. Markers indicate the locations of the scaled eigenvalues. Notice that these choices of h_t are (approximately) the largest such that the scaled eigenvalues fall inside the stability region.

Parameter Name (Description)	Set of Values
c (advection coefficient/speed)	1
ν (diffusion coefficient)	0, 1×10^{-4} , and 1×10^{-2}
P (period)	1
p (decay rate of Fourier series coefficients of initial data)	2, 4, 8
N (number of computational nodes in S)	51, 101, 201
n (number of nearest neighbors)	3, 5, 7, 9, 11
s (steps in multi-step method)	2 and 3
h_t (time step in numerical integration)	$h_{t,N,\nu,s}$, $1.01h_{t,N,\nu,s}$, $1.1h_{t,N,\nu,s}$
Q (number of recurrent steps in loss)	1, 3, 4, 5, 9
T (number of training cases)	1, 10, 100
κ_{\max} (maximum number of iterations in quasi-Newton method)	10, 100, 1000

Table 3: Parameter sets

since a goal here is to determine whether minimizing J can deliver a stable method for values of N , h_t , ν and s where traditional methods may fail. Table 3 includes all parameter values used in this study, and each possible combination (for a total of 36450) computational experiments were performed. Further, in all cases the vector of weights is initialized as

$$\boldsymbol{\omega}^{(0)} = [(\mathbf{w}'_1)^T \quad (\mathbf{w}'_2)^T]^T$$

for the quasi-Newton method. Other choices of initial weight vectors are certainly possible, but this choice provided the most success in constructing stable methods for the combinations of parameters listed in table 3.

Once weights are computed by minimizing J , they are utilized to approximate the solution to (1) for $t \in (0, 20]$ and $x \in [0, 1)$ beginning with initial data defined from the partial sum

$$u(x, t) = \sum_{\eta=-300}^{300} b_{\eta}(0) e^{i \frac{2\pi\eta}{P}(x-ct) - \left(\frac{2\pi\eta}{P}\right)^2 \nu t}, \quad (17)$$

with $t = 0$ and $b_{\eta}(0)$ chosen to be the coefficients of the 1-periodic ($P = 1$) extension of the bump function,

$$u_0(x) = \begin{cases} e^{\frac{1}{(2(x-\lfloor x \rfloor)-1)^2-1}}, & x \notin \mathbb{Z} \\ 0, & x \in \mathbb{Z} \end{cases}. \quad (18)$$

These values of $b_{\eta}(0)$ are computed numerically from (3) using Matlab's (R2022b) integral function with `AbsTol` set to `eps`. The modulus of $b_{\eta}(0)$ decreases with

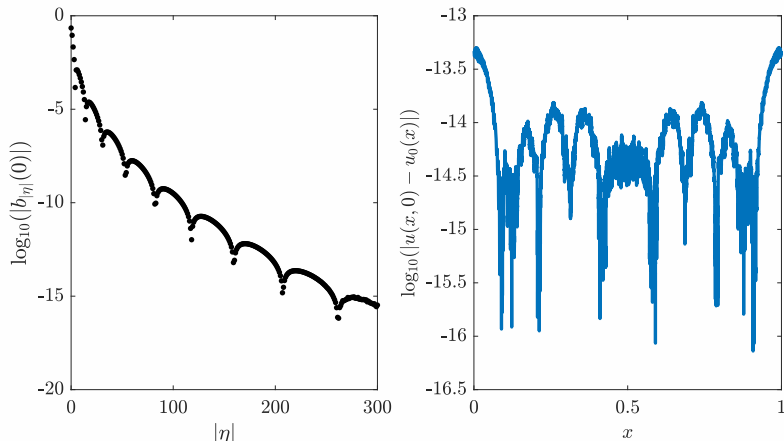


Figure 3: Left: modulus of $b_n(0)$ for the bump function (18). Right: log base 10 of the error in the approximation (17) of (18).

the modulus of η , although not monotonically, and reaches machine precision (near 10^{-16}) when $|\eta| \approx 300$. This coincides with the initial data being continuous and smooth in the sense that all of its derivatives are continuous as well. An illustration of these coefficients and the absolute difference between $u(x, 0)$ from (17) and $u_0(x)$ from (18) is shown in figure 3. Notice that for this initial data, exact solutions to (1) are given by (17). Therefore, to evaluate the forward error in the approximate solution, the vector $\mathbf{u}(t)$ is constructed at discrete values of t , equally spaced by h_t , defined entrywise as $[\mathbf{u}(lh_t)]_k = u(x_k, t)$ with u as in (17) and for $l \geq 0$. Further, to kickstart the AB- s method (9), it is useful to set $\tilde{\mathbf{u}}(lh_t) = \mathbf{u}(lh_t)$, $l = 0, 1, \dots, s-1$. It should also be noted that this initial data is not contained in the training data for any of $p = 0, 2, 8$.

9 Key Observation on Recurrent Loss and Stability

The experiments outlined in section 8 are intended, in part, to assist in understanding the mechanism by which recurrent loss can promote stability in the numerical solution of a PDE. Remarkably, without imposing any explicit conditions on the spectrum of the matrix D , minimizing J results in a set of eigenvalues such that $\{\lambda_\eta h_t\}_{\eta=-\lfloor N/2 \rfloor}^{\lfloor N/2 \rfloor}$ (with λ_η as in (7)) adapts, to some extent, to the stability region of the multi-step method under consideration. In some cases, the weights in D are altered in such a way that the set of scaled eigenvalues falls entirely within the stability region, resulting in a stable method. The

dependence of the adaptation of the scaled eigenvalues to the stability region (and stability characteristics of the resulting numerical method) on the various parameters discussed in section 8 is complicated, with no discernible patterns arising. The remainder of this section discusses observations relative to Q , T , κ_{\max} , p , and N .

Consider figure 4, with the rows of plots corresponding to different values of κ_{\max} , increasing from top to bottom. The left column of subplots displays log base 10 of the infinity norm absolute forward error in the numerical solution computed using the weights generated by minimizing J . The colors indicate varying values of Q and the curve styles depict different values of T . The remaining parameter values are given in the figure title. Similarly, the right column of subplots depicts the eigenvalues of D , constructed from these weights, with markers this time indicating different values of T . In all of the rows, the black curves in the left column and the black dots in the right column correspond to the absolute forward error and eigenvalues, respectively, of the second order centered difference method (with corresponding matrix D'). Here $\nu = 0$ and $s = 2$ so that second order centered difference method is unstable for any value of $h_t > 0$. However, even for $h_t = 1.10h_{t,N,\nu,s}$ weights for approximating the action of \mathcal{L} can be determined for which the overall numerical method is stable. This can be seen in the third row of subplots. Since the second order centered difference method is unstable, the error increases exponentially, even for $t \ll 1$, with a rate dependent on the size of certain eigenvalues for which $\lambda_\eta h_t$ falls outside of the stability region. Through the minimization of J over $\kappa_{\max} = 1000$ iterations of the quasi-Newton method, two sets of weights are determined for which the forward error in the solution remains well below 10^{-1} for all $lh_t \in [0, 20]$, $l > 0$. Referring to the corresponding sets of eigenvalues in the bottom right subplot, those sets of parameters corresponding to stable solutions also produce sets of eigenvalues so that $\lambda_\eta h_t$ falls entirely inside the stability region. For example, consider the error curve and corresponding eigenvalues when $Q = 1$ and $T = 10$ or when $Q = 9$ and $T = 1$.

Noticeably, improvements in stability are not predictably guaranteed by increasing Q or T . Considering the choice of Q , the first row of plots in figure 4 demonstrates what could hopefully be expected. That is, as Q increases, it might be expected that the values of t for which the growth in $\|\mathbf{u}(t) - \tilde{\mathbf{u}}(t)\|_\infty$ transitions from polynomial to exponential also increases. This is a general trend in the first row; however, here there are even departures with, for example, $Q = 5, 7$ violating the trend with respect to $Q = 3$ when $T = 1$. Further, with increasing κ_{\max} (in the second and third rows the figure) the trend seems to break down entirely with a set of weights for $\kappa_{\max} = 1000$ generated with $Q = 1$ (also with slightly more training data) even performing marginally better than that of $Q = 9$. Likewise, as T increases it might be expected that computed weights converge to a particular set of values. However, each row of figure 4 does not provide evidence that this is the case. There are clearly combinations of T and Q for which the $T = 1$ and $T = 100$ cases perform more alike than the $T = 10$

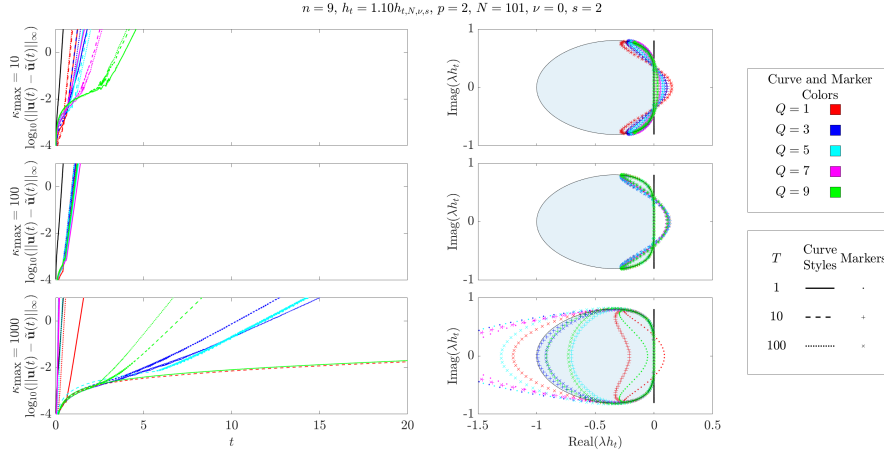


Figure 4: Left column: log base 10 of the infinity norm absolute forward error in the numerical solution computed using the weights generated by minimizing J . The colors indicate varying values of Q and the curve styles depict different values of T . The remaining parameter values are given in the figure title. Right column: eigenvalues of D , constructed from these weights, with markers this time indicating different values of T . Rows correspond to different values of κ_{\max} , increasing from top to bottom. In all of the rows, the black curves in the left column and the black dots in the right column correspond to the absolute forward error and eigenvalues, respectively, of the second order centered difference method (with corresponding matrix D'). Parameter choices are indicated in the title of the plot. Notice that increases in Q , the number of time steps included in the recurrent loss function, do not predictably improve stability. Similarly, performance relative to increases in T , the number of training samples, is erratic.

case (see, for instance the curves for $Q = 1$ in the bottom row). Now, it is likely that the choices of T explored here are not large enough to demonstrate such convergence; however, if the convergence is to a set of weights for which the method for solving (1) is unstable or low accuracy, then there is no benefit to consider even larger values of T . Still, the extent to which the values of $\lambda_{\eta}h_t$ are conforming to the boundary of the stability region is notable in all cases.

Changing ν from 0 to 10^{-4} leads to a case where there is a maximum value $h_t = h_{t,N,\nu,s}$ for which AB-2 is stable. Leaving all other parameters the same as those used in the results presented in figure 4, figure 5 highlights even more unpredictable behavior, but relative to κ_{\max} . It should be expected that the weight set computed using the quasi-Newton method converges superlinearly to a stationary point of J (see, e.g., [22]). The rows of subplots in figure 5 demonstrate that, while minimization of the forward error in $\tilde{\mathbf{u}}(lh_t)$ for $l = 1, 2, \dots, Q$

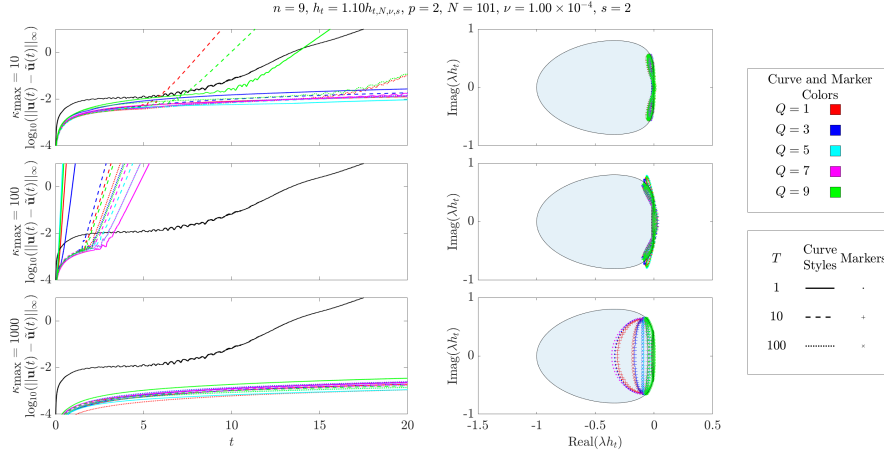


Figure 5: See figure 4 for a discussion of what is depicted in each subplot. Parameter choices are indicated in the title of the plot. Notice that a systematic method choosing κ_{\max} to produce weights for a stable numerical method may not exist.

simultaneously can promote both stability and improved accuracy, the number of iterations κ_{\max} required to achieve these improvements is uncertain. That is, in this case the choices of $\kappa_{\max} = 10$ and $\kappa_{\max} = 1000$ produce many sets of weights for which the numerical method is both accurate and stable, while the choice of $\kappa_{\max} = 100$ does not produce any. One benefit of increasing κ_{\max} in this particular case is that many of the combinations of Q and T for which sets of weights are found that lead to accurate and stable solutions actually achieve lower forward error when increasing from $\kappa_{\max} = 10$ to $\kappa_{\max} = 1000$. This is precisely what one should hope for; however, once a set of weights is found for which the method is stable, additional iterations in the minimization of J still attempt to reduce the error, but only over the Q steps under consideration. This can often lead to methods that are more accurate over the short time horizon (i.e., $t = lh_t, l = 1, 2, \dots, Q$ only), yet unstable for larger κ_{\max} although fewer iterations of the quasi-Newton method return accurate and stable methods. An example of this undesirable behavior is given in figure 6.

The value of p , which impacts the behavior of the initial data (that is, $b_{|\eta|}(0) = O(\eta^{-p})$ as $\eta \rightarrow \infty$), is chosen to mimic varying degrees of smoothness of the initial data. As p increases the contribution of $\mathbf{v}_{|\eta|}$, $|\eta| > 1$, in (8) diminishes. Further, the eigenvalues (7) corresponding to larger $|\eta|$ typically have modulus that is larger than those for small $|\eta|$. That is, $\lambda_{\eta} h_t$ is more likely to fall outside of the stability region of the AB- s method for larger $|\eta|$ than for small. Therefore, the diminished influence of these eigenvectors discounts the influence of the corresponding eigenvalues on instability, particularly for the small values

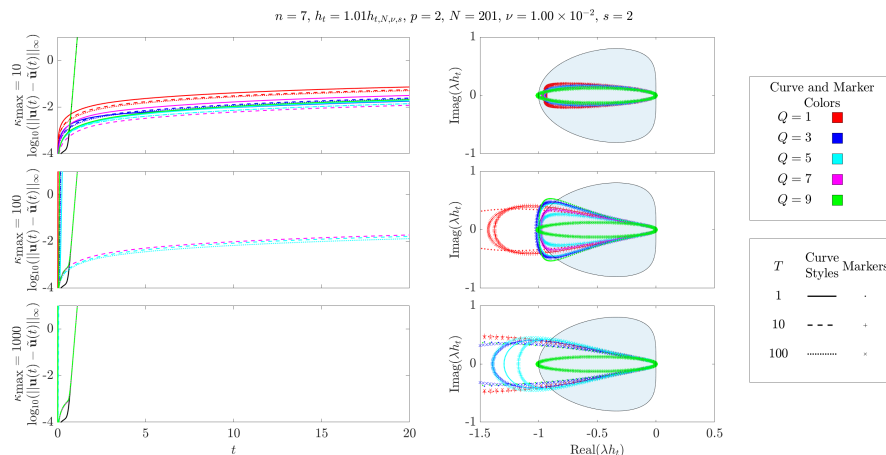


Figure 6: See figure 4 for a discussion of what is depicted in each subplot. Parameter choices are indicated in the title of the plot. Notice that increases in κ_{\max} do not guarantee convergence to weights for a stable numerical method, even when smaller values of κ_{\max} produced such sets.

of t considered in the process of minimizing J . Practically speaking, this has translated to fewer combinations of s, n, ν, N and h_t for which any weight sets leading to a stable method being generated as p increases since the objective detects less growth from the scaled eigenvalues outside the stability region. Still, figure 7 demonstrates what can be lost when choosing p too low. Comparing to figure 5, the only parameter that has changed is the value of p . Unsurprisingly, when the eigenvalues that fall outside the stability region are given more emphasis in the case of $p = 0$ (figure 7) the accuracies of the resulting numerical methods appear to suffer in comparison to the $p = 2$ case (figure 5) since the minimization of J must contend with the instability to a greater extent, impacting further improvements in accuracy.

Figure 8 is generated from the same parameter set as figure 5 except that N is increased from 101 to 201. Notice that in this case, the solutions illustrated in the results of the numerical methods in the case of $N = 201$ appear more accurate than those when $N = 101$. Further, weights generating stable numerical methods are found when $N = 201$ and $\kappa_{\max} = 100$ but not for $N = 101$ and the same value of κ_{\max} . Increases in the node set size, N , lead to smaller values of $h_{t,N,\nu,s}$ required for the centered difference method to be stable (excluding the case of $s = 2$ and $\nu = 0$); however, the centered difference is also more accurate for larger N . Figures 5 and 8 hint that the same behavior may be possible for numerical methods utilizing the weight sets constructed by minimizing J . Unfortunately, except in rare cases like the one depicted here, increases in N do not reliably lead to the determination of weights that promote stability or

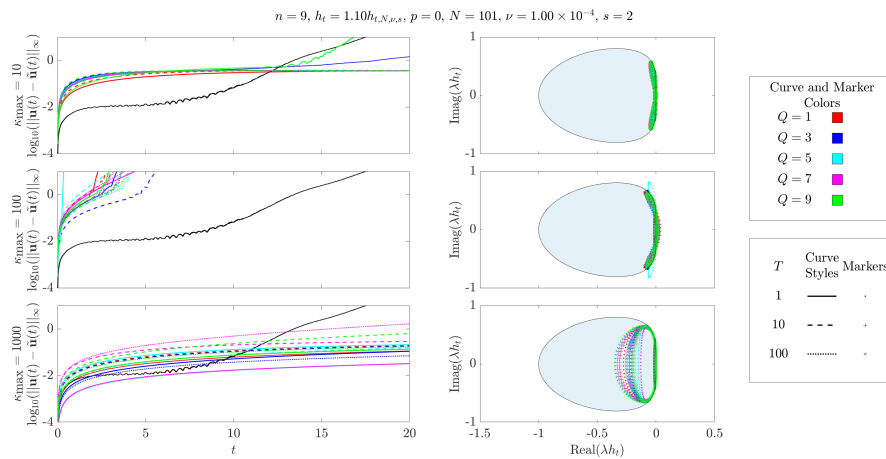


Figure 7: See figure 4 for a discussion of what is depicted in each subplot. Parameter choices are indicated in the title of the plot. The impact of the decay of the coefficients in the initial data is demonstrated here when compared to figure 5. Deemphasising the eigenvalues of larger modulus that fall outside the stability region for the centered difference method can limit the possibility of determining weights for a stable method. Overemphasis of these eigenvalues can limit the accuracy in the resulting numerical method.

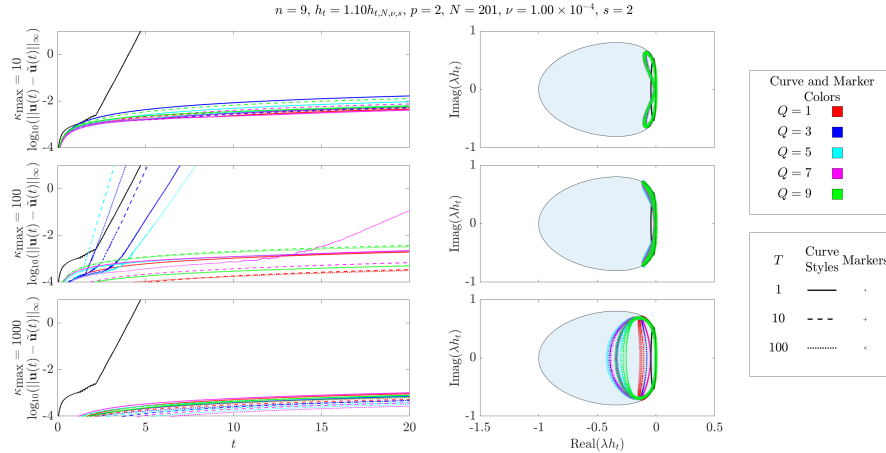


Figure 8: See figure 4 for a discussion of what is depicted in each subplot. Parameter choices are indicated in the title of the plot. When compared to figure 5 it might be concluded that increases in N lead to weight sets that promote greater stability and accuracy. Unfortunately, except in rare cases like those depicted here, this is not the case.

greater accuracy in the resulting numerical methods.

10 Other Significant Observations

In the absence of a concise visual representation of all of the data collected, further observations on the performance of this approach for generating weight sets for approximating the spatial derivative operators when solving the advection-diffusion equation are collected here.

- When $p = 8$, the weight sets generated for $n = 3$ deviate little from those in D' . The weights in D' are constructed to have low truncation error at each step, specifically in the case of $n = 3$. Attempts to decrease $J_{\tau q}$, and thus J , in this case are more difficult as the initial guess for the quasi-Newton method, which is the weight set used in D' , is already likely at or near a local minimum of J . It may be possible to determine weights that both deviate from those in D' and improve upon the value of J ; however, there is no clear systematic way to determine initial guesses that would do so.
- In line with the previous observation, generation of weight sets that are both more accurate and stable appears more likely as n increases. This

should be expected as the search space increases in size.

- Increases in h_t beyond $h_{t,N,\nu,s}$ inflate the number of scaled eigenvalues of D' that fall outside the stability region while also increasing their modulus. Therefore, in practice the number of weight sets that are found that lead to stable numerical methods decreases with the increases in h_t examined here. This is unfortunate as it would be desirable to determine weight sets for which stability is possible even for large values of h_t to improve the efficiency of numerical simulation.
- While there is a maximum value of h_t for which the centered difference method is stable for each choice ν when $s = 3$ (but not for $s = 2$), this approach to constructing weight sets that lead to stable numerical methods is more successful when $s = 2$. Figure 2 illustrates that the area of the stability region of AB-3 is larger than that of AB-2, which may account for the greater success. However, this has not been systematically verified. Further, AB-3 is a more accurate method than AB-2 and the discussions on accuracy above should analogously apply here.

11 Conclusions

The computational results presented in sections 9 and 10 demonstrate that stable solutions of the advection-diffusion equation can be found through the minimization of a recurrent loss function even for parameter sets where traditional numerical methods may fail. However, the observations of the same sections highlight an important difficulty with data-driven approaches to solving PDEs—the results can be unpredictable. The PDE and network model used here can be fully characterized, with known exact solutions to the PDE and with weights in the network that can be easily interpreted as entries in a matrix that represents a discrete approximation of a linear operator. Yet, even in this simplified case, the results do not suggest the existence of a reliable and robust set of criteria for constructing weight sets that lead to stable numerical methods for solving (1). Most importantly, it does not appear that increasing any of

- the number of time steps included in the recurrent loss,
- the smoothness of the initial data,
- the amount of training data, or
- the number of iterations in the optimizations method

has a predictable impact on determining a desirable set of weights.

Still, the successes demonstrated here are worth further investigation, and there are many opportunities for further research into stable numerical methods for

time-dependent PDEs that rely on the techniques of machine learning. Some of these include

- approaches for the selection of initial weight vectors for the quasi-Newton method
- consideration of entirely different methods of optimization like steepest descent (see, e.g., [22])
- characterization of the size of, e.g., $\delta_{\tau q}^C(lh_t; \omega)$, as Q increases and for different value of l to identify potential vanishing gradients
- alternative network architectures, like long short-term memory (LSTM) [23], in the case of vanishing gradients
- allowance for the multi-step weights α_l to also vary in the process of minimizing J .

References

- [1] Arieh Iserles. *A First Course in the Numerical Analysis of Differential Equations*. Cambridge Texts in Applied Mathematics. Cambridge University Press, 2 edition, 2008.
- [2] Y. Bar-Sinai, S. Hoyer, J. Hickey, and M. P. Brenner. Learning data-driven discretizations for partial differential equations. *Proceedings of the National Academy of Sciences*, 116(31):15344–15349, 2019.
- [3] Kristina O. F. Williams and Benjamin F. Akers. Numerical simulation of the korteweg–de vries equation with machine learning. *Mathematics*, 11(13), 2023.
- [4] Benjamin F. Akers and Kristina O. F. Williams. Coarse-gridded simulation of the nonlinear schrödinger equation with machine learning. *Mathematics*, 12(17), 2024.
- [5] Zichao Long, Yiping Lu, Xianzhong Ma, and Bin Dong. PDE-net: Learning PDEs from data. In Jennifer Dy and Andreas Krause, editors, *Proceedings of the 35th International Conference on Machine Learning*, volume 80 of *Proceedings of Machine Learning Research*, pages 3208–3216. PMLR, 10–15 Jul 2018.
- [6] Z. Chen, V. Churchill, K. Wu, and D. Xiu. Deep neural network modeling of unknown partial differential equations in nodal space. *J. Comput. Phys.*, 449(C), jan 2022.

- [7] Maziar Raissi. Deep hidden physics models: deep learning of nonlinear partial differential equations. *J. Mach. Learn. Res.*, 19(1):932–955, January 2018.
- [8] M. Raissi, P. Perdikaris, and G.E. Karniadakis. Physics-informed neural networks: A deep learning framework for solving forward and inverse problems involving nonlinear partial differential equations. *Journal of Computational Physics*, 378:686–707, 2019.
- [9] Zichao Long, Yiping Lu, and Bin Dong. Pde-net 2.0: Learning pdes from data with a numeric-symbolic hybrid deep network. *Journal of Computational Physics*, 399:108925, 2019.
- [10] Jan Nordström and Oskar Ålund. Neural network enhanced computations on coarse grids. *Journal of Computational Physics*, 425:109821, 2021.
- [11] Warren Mcculloch and Walter Pitts. A logical calculus of ideas immanent in nervous activity. *Bulletin of Mathematical Biophysics*, 5:127–147, 1943.
- [12] D. E. Rumelhart, P. Smolensky, J. L. McClelland, and G. E. Hinton. Schemata and Sequential Thought Processes in PDP Models. In *Parallel Distributed Processing, Volume 2: Explorations in the Microstructure of Cognition: Psychological and Biological Models*. The MIT Press, 07 1986.
- [13] Pinchao Meng, Xinyu Wang, and Weishi Yin. Ode-ru: a dynamical system view on recurrent neural networks. *Electronic Research Archive*, 30(1):257–271, 2022.
- [14] W. Ee. A proposal on machine learning via dynamical systems. *Commun. Math. Stat.*, 5:1–11, 2017.
- [15] Eldad Haber, Keegan Lensink, Eran Treister, and Lars Ruthotto. IMEXnet a forward stable deep neural network. In Kamalika Chaudhuri and Ruslan Salakhutdinov, editors, *Proceedings of the 36th International Conference on Machine Learning*, volume 97 of *Proceedings of Machine Learning Research*, pages 2525–2534. PMLR, 09–15 Jun 2019.
- [16] E. Haber and L. Ruthotto. Stable architectures for deep neural networks. *Inverse Problems*, 34(1), 2017.
- [17] R. B. Guenther and J. W. Lee. *Partial Differential Equations of Mathematical Physics and Integral Equations*. Dover Publications, Inc., 1996.
- [18] J.K. Hunter and B. Nachtergaele. *Applied Analysis*. World Scientific, 2001.
- [19] K. E. Atkinson. *An Introduction to Numerical Analysis*. John Wiley & Sons, 2nd edition, 1989.
- [20] Randall J. LeVeque. *Finite Difference Methods for Ordinary and Partial Differential Equations*. Society for Industrial and Applied Mathematics, 2007.

- [21] Michelle Ghrist, Bengt Fornberg, and Jonah Reeger. Stability ordinates of adams predictor-corrector methods. *BIT Numerical Mathematics*, 55, 12 2014.
- [22] J. Nocedal and S. J. Wright. *Numerical Optimization*. Springer, 2nd edition, 2006.
- [23] Sepp Hochreiter and Jürgen Schmidhuber. Long short-term memory. *Neural Computation*, 9:1735–1780, 11 1997.